Bulletin of the Seismological Society of America, Vol. 70, No. 4, pp. 1055–1070, August 1980

MICROSEISMS: A TWENTY-SIX-SECOND SPECTRAL LINE IN LONG-PERIOD EARTH MOTION

BY L. GARY HOLCOMB

ABSTRACT

A narrow-band microseismic peak exists in worldwide earth background near a period of 26 sec. During storms, the amplitude of this ground motion increases to high levels which allows detailed studies of its characteristics. Analysis indicates that the energy arrives as Rayleigh waves from a source in the southern Atlantic Ocean. The most significant property of this microseismic peak is that it is nondispersive, thereby eliminating deep-water ocean-wave dispersion as the mechanism for isolating the narrow-band energy.

INTRODUCTION

The study of microseisms spans the history of seismology, and the accumulated literature is as massive as that on any particular aspect of seismology (see, e.g., Iyer, 1964). The first microseism peak to be discovered and studied consisted of what is commonly referred to as the 7-sec microseism peak. Later, as longer period instrumentation became available, the 18-sec microseisms were studied, and harmonic relationships between the two peaks were proposed (Oliver and Page, 1963). The microseismic background beyond 20 sec has not received much attention. However, Oliver (1962, 1963) reported a rare storm of microseisms with a 27-sec period, which was observed worldwide. This storm was so vigorous that the microseisms could be seen on analog records at several stations. Oliver attributed the storm to long-period ocean waves impacting on the African coast bordering on the Gulf of Guinea. These ocean waves were believed to have originated in a severe meteorological disturbance located somewhere in the South Atlantic. Later, Haubrich *et al.* (1963) reported observations of microseisms with periods of approximately 25 sec, which they deduced were generated on the southern California coastline by ocean waves traveling all the way from the Ross Sea near the Antarctica continent.

During the past 4 yr, the power spectra of a large amount of long-period seismic background data as recorded at the Albuquerque Seismological Laboratory have been analyzed during the evaluation and testing of the new long-period borehole seismometer systems that are being used at the seismic research observatories (SRO). This analysis established that long-period earth motion, similar to that reported by Oliver, occurred at Albuquerque quite frequently. This observation aroused enough curiosity to promote a more detailed study of that portion of the spectrum. As data from newly installed SRO stations became available from around the world, the same type of microseismic peak was also observed much of the time at the new stations. It became evident that Oliver's "storm" of long-period microseisms was not an isolated case. Earth motion of this general nature occurs worldwide as a more or less continuous background, which occasionally increases dramatically in isolated storms in much the same manner as the 7- and 18-sec peaks behave.

TWENTY-SIX-SECOND BACKGROUND

The ambient 26-sec earth motion is much too small to be observed on time-domain analog records. To date, the current study has not revealed an extraordinary storm strong enough to be seen visually on the analog records as reported by Oliver.

However, both ambient background and smaller storms are readily observed in power spectra of long-period data.

All of the power spectra presented here were obtained as follows: the data originally recorded at one sample per second were first decimated by a factor of 2, then a 2048-point Fast Fourier transform was obtained using a rectangular window. The power spectra as calculated from the transform were frequency smoothed over nine frequencies (Bendat and Piersol, 1971). The low degree of smoothing yields a rather ragged power spectral density curve but is necessary in order to resolve the peak of the 26-sec energy, which is sometimes a remarkably sharp line. Figure 3 contains further smoothing by segmented averaging.

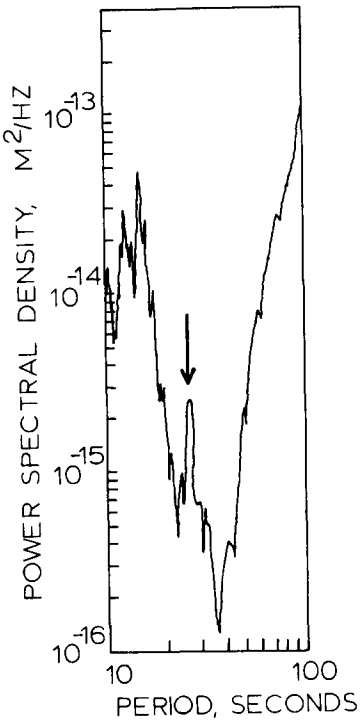

FIG. 1. Background earth motion conditions at ANMO showing a typical level of the 26-sec microseism peak (arrow). Data from 7,158,06:23:00.

Figure 1 is typical of the approximate level of the 26-sec microseisms in the background power spectra, whereas Figure 2 shows a time period during which the peak was absent. Small peaks in the microseismic background at about this period are present quite frequently at stations worldwide. The amplitude varies from hour to hour and the peaks frequently disappear below the background noise level for considerable lengths of time. There does not appear to be any correlation in the time of occurrence of the ambient peaks or in their amplitudes at stations spaced on the worldwide scale. These factors make it very difficult to determine a source for the ambient energy.

TWENTY-SIX-SECOND STORM CHARACTER

Occasionally, the amplitude of this microseism peak increases dramatically. In particular, a storm (The term "storm" as used in this paper, refers to microseismic earth motion that is significantly larger than normal; no connection with atmospheric

storms is implied.) beginning on June 8, 1977, illustrates the characteristics of storm data. This storm, which lasted approximately 72 hr at Albuquerque, was observed by SRO, Upgraded High-Gain Long-Period Stations (ASRO), and High-Gain Long-Period (HGLP) stations throughout the world. Figure 3 contains the vertical, north-south, and east-west power spectra for a common $4\frac{1}{2}$-hr period during the height of the storm from all of the stations in operation at that time.

The presence of the 26-sec microseism peak is readily apparent in the power spectra from ALQ, ANMO, EIL, KON, OGD, and MAIO (see Table 1 for definition of station codes and geographic locations). Closer inspection reveals that it appears in all of the stations with the possible exception of SNZO. The SNZO SRO was

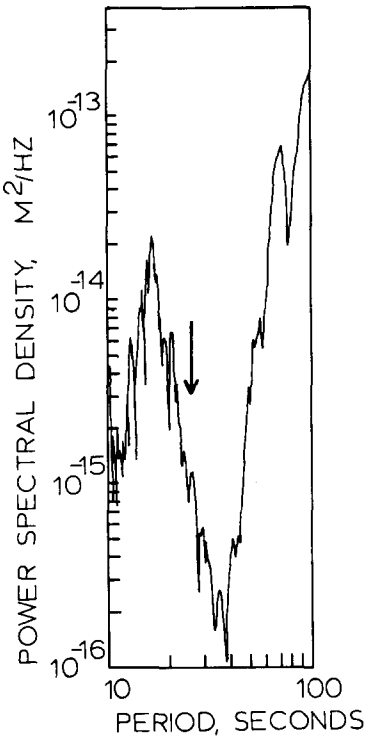

FIG. 2. Background earth motion conditions at ANMO in which the 26-sec microseism peak (arrow) is not evident. Data from 7,164,06:35:00.

excessively noisy; the noise may be hiding the small 26-sec peak. The remarkable aspect of the power spectral density data shown in Figure 3 is the narrow bandwidth of the microseism peak. It is much narrower than the typical 18-sec microseism peak, and the period at which it reaches its maximum is strikingly uniform at all stations for all components worldwide, as Table 2 illustrates. All observed peak maxima in Figure 3 fall within 0.5 sec of 26 sec.

Power level histories of the 26-sec peak in the spectral density functions at ANMO, EIL, KON, MAIO, and OGD are contained in Figure 4. The general shape of the power histories is quite similar for all five stations. Ground motion amplitude increases rapidly in the first three-quarters of a day; then it slowly dies off during the next 3 days. (This type of behavior is also typical of the time dependence of the ground motion generated by 18-sec storms.) The uniformity of the period of the peaks coupled with the similarity of the power histories leaves little doubt that a common source generated the energy that was recorded worldwide.

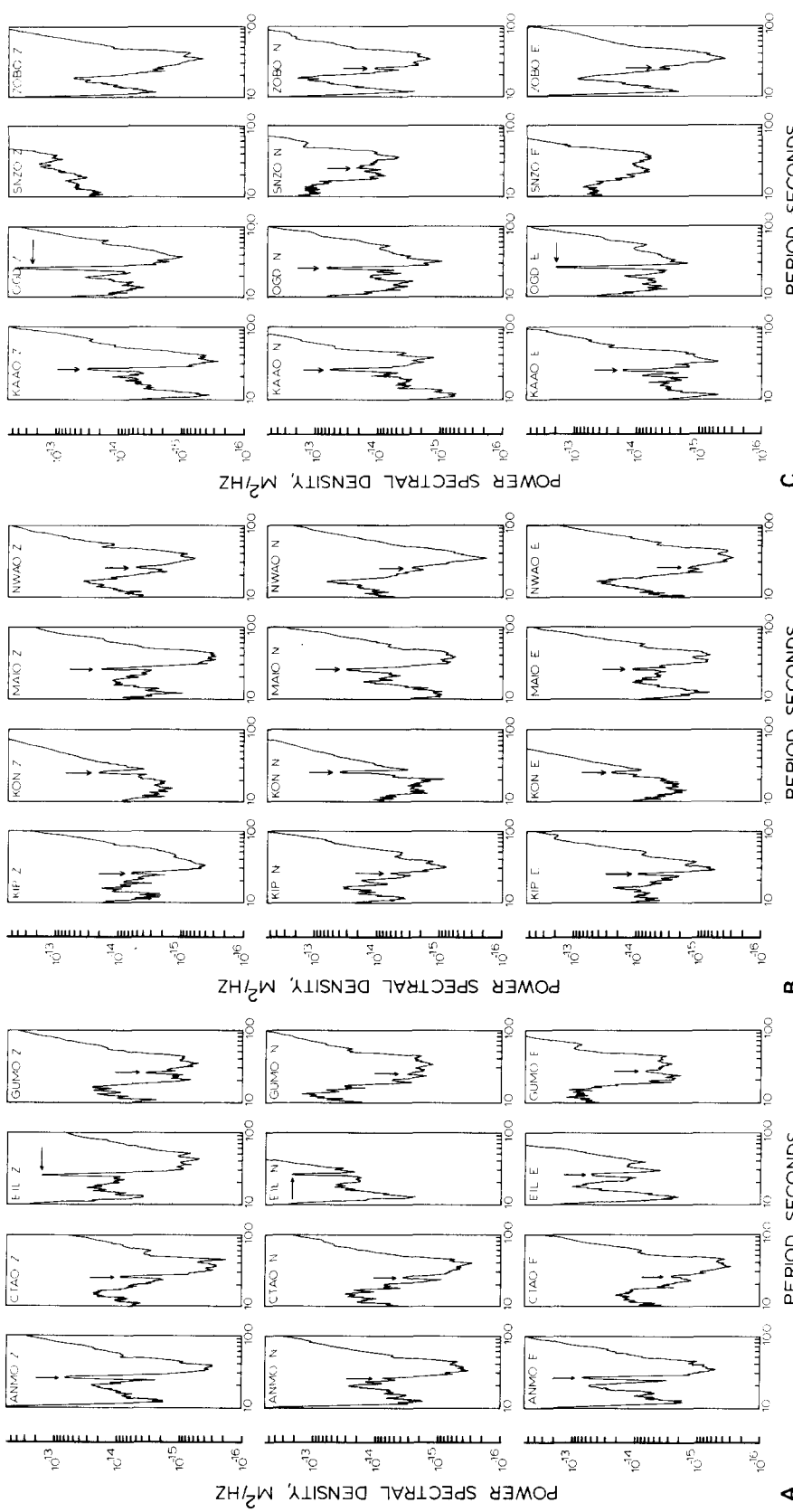

FIG. 3. Three-component power spectra during the 26-sec microseismic storm of June 8, 1977. Each plot represents 4½ hr of data starting at 7,159,08:00:00, obtained by averaging four segments (arrow denotes 26-sec peak). The periods at which the individual peaks occur are listed in Table 2.

Storm Source Location

Determining the geographic source of the 26-sec energy is not a straightforward task. Microseismic storms have no sudden onsets which can be used for travel-time origin determination. The literature on microseisms contains descriptions of many different methods for determining the direction of arrival of microseismic energy. The most commonly used method is referred to as particle motion studies, in which the arriving energy is assumed to be a simple Rayleigh wave, and the direction of arrival is determined by earth particle motion in the horizontal plane. However, numerous studies have shown that the energy does not arrive in the form of pure Rayleigh waves (Evernden, 1953, 1954). It is commonly believed that the energy is a combination of both Rayleigh and Love waves or that the total particle motion at a given site results from the sum of Rayleigh waves arriving at the station from several directions simultaneously. The latter theory explains the appearance of the beats which are always observed in microseismic time-domain data.

A combination of three different methods was used to determine the azimuths of the arriving 26-sec microseisms. They will be referred to as the particle motion method, the amplitude spectrum method, and the cross spectrum method.

TABLE 1

Station Codes and Geographic Locations

Code	Station	Type	Latitude	Longitude
ALQ	Albuquerque, New Mexico	HGLP	34°56'33.0"N	106°27'27.0"W
ANMO	Albuquerque, New Mexico	SRO	34°56'33.0"N	106°27'27.0"W
CTAO	Charters Towers, Australia	ASRO	20°05'18.0"S	146°15'16.0"E
EIL	Eilat, Israel	HGLP	29°33'00.0"N	34°57'00.0"E
GUMO	Guam, Mariana Islands	SRO	13°35'16.0"N	104°51'58.6"E
KAAO	Kabul, Afghanistan	ASRO	34°32'27.0"N	69°02'35.4"E
KIP	Kipapa, Hawaii	HGLP	21°25'24.0"N	158°00'54.0"W
KON	Kongsberg, Norway	HGLP	59°38'56.7"N	9°35'53.6"E
MAIO	Mashhad, Iran	SRO	36°18'00.0"N	59°29'40.2"E
NWAO	Mundaring, Australia	SRO	32°55'37.0"S	117°14'02.0"E
OGD	Ogdensburg, New Jersey	HGLP	41°05'15.0"N	74°35'45.0"W
SNZO	Wellington, New Zealand	SRO	41°18'37.0"S	174°42'16.7"E
ZOBO	La Paz, Bolivia	ASRO	16°16'12.0"S	68°07'30.0"W

Particle Motion Azimuths

Particle motion studies of the ANMO, OGD, KON, EIL, and MAIO data were made by first digitally filtering the data through a bandpass of from 25 to 30 sec. Then analog time records of the filtered Z, N, and E components were visibly inspected to find time periods during which the horizontal and vertical components best approximated Rayleigh wave motion.

As an example of the results of visual particle motion of the 26-sec storm data, a section of the bandpass-filtered analog record from Ogdensburg, New Jersey, is shown in Figure 5. Ogdensburg data displayed remarkable Rayleigh wave character throughout the duration of the storm. Inspection of Figure 5 reveals that the vertical component is nearly 90° ahead of the north-south and that the east-west is approximately 180° out of phase with the north-south; this indicates that the Rayleigh waves arrived from the southeast quadrant at Ogdensburg. The results of visual particle motion studies of data from ANMO, EIL, KON, MAIO, and OGD are tabulated in Table 3. The Rayleigh wave character at the other four stations is not as high as at Ogdensburg, but it is good enough that the indicated quadrants are

believed to be reliable. The amplitude of the 26-sec ground motion in the data from the remaining seven stations is too small to allow particle motion analysis. The particle motion data of Table 3 indicate a source region lying east of Ogdensburg, New Jersey, west of Kongsberg, Norway, and south of Eilat, Israel. It is not possible to be more precise due to the few stations available in the Southern Hemisphere around the Atlantic Ocean.

Amplitude Spectrum Azimuths

The second method of determining the direction of arrival of the microseismic energy appears in the literature of adaptive filters (Simons, 1968). Basically, the approach utilizes the ratio of the amplitude spectrum of the horizontal components

TABLE 2

Periods at Which the Maximum in the 26-Sec Microseism Peak Occurred at All Stations for Each Component. Data Obtained from Power Spectral Density Analysis of Data from a Simultaneous 4-Hr Time Period Starting at 7,159,08:00:00, Except for the Data from KAAO, Which Start at 7,159,11:00:00.

Station	Vertical	North	East
ALQ	26.43	25.92	26.43
ANMO	26.43	25.92	26.43
CTAO	25.76	25.76	26.09
EIL	26.09	26.09	26.09
GUMO	26.43	26.09	26.43
KAAO	26.43	26.26	26.26
KIP	26.26	26.09	26.26
KON	26.09	26.09	25.60
MAIO	26.60	26.09	26.09
NWAO	26.43	26.09	25.92
OGD	26.43	26.26	26.26
SNZO	~*	25.92	~
ZOBO	26.46	26.26	26.26

* ~, no data.

to determine the azimuth of arrival of pure Rayleigh waves. First, calculate the amplitude coefficients of the Fourier transform for the north and east components for a common time period from

$$A_N(P) = \sqrt{R_N^2(P) + I_N^2(P)}, \quad \text{and} \quad A_E(P) = \sqrt{R_E^2(P) + I_E^2(P)}, \tag{1}$$

where R_N, I_N and R_E, I_E are the real and imaginary components of the Fourier transform of the time series of the north and east components at period P. Then, if the energy arrives in the form of Rayleigh waves and the sensitivities of the north-south and east-west components are equal, one of the four possible azimuths of the arrival is given by

$$\alpha(P) = \tan^{-1} \frac{A_E(P)}{A_N(P)}, \tag{2}$$

and the other three possible directions are $360 - \alpha$, $180 - \alpha$, and $180 + \alpha$. Determining the direction of arrival using the amplitude spectrum method is much more precise

than the particle motion approach because of the averaging effect of analyzing data obtained over an extended period of time as opposed to data analysis confined to a few cycles. The longer time base tends to eliminate the influence of energy arriving from different directions, thereby indicating a mean direction of arrival.

Approximately $4\frac{1}{2}$ hr of data were analyzed from a common time period, and the azimuths of arrival as given by equation (2) were calculated at all stations. Using the particle motion results from ANMO, EIL, KON, MAIO, and OGD to assist in resolving the four-angle ambiguity of equation (2), and assuming a great circle travel path, a region off the southwestern coast of Africa is indicated as the source of the 26-sec energy. Table 4 compares the azimuths calculated from the data with the great circle azimuth from each of the stations to the point defined by latitude 32° S, and longitude 9° E. This trial-and-error-determined point agrees very well with the azimuths calculated for ANMO, ALQ, CTAO, EIL, KIP, MAIO, and OGD. The errors are greater for KON, NWAO, and ZOBO, but they still indicate that the

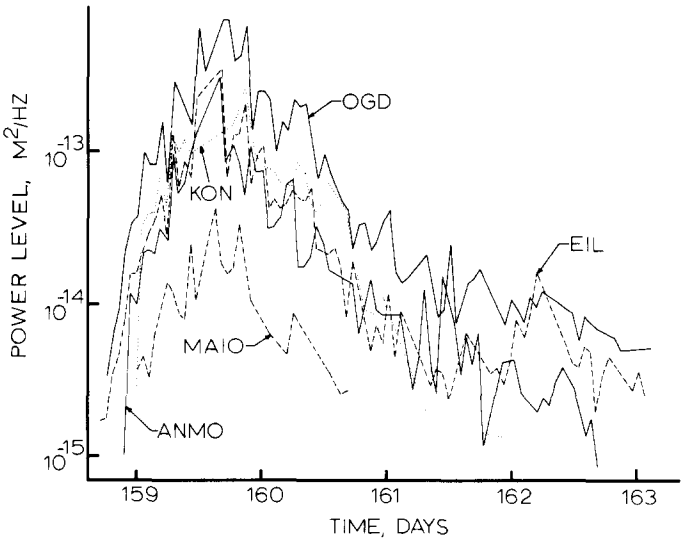

FIG. 4. Power level histories of the 26-sec microseism peak at ANMO, EIL, KON, MAIO, and OGD.

energy originated in approximately the same area. The spectral line in data from GUMO and SNZO is not of sufficient amplitude to determine arrival direction reliably; in addition, arrival azimuths at KAAO are not consistent. It is noteworthy that both independent systems operating at Albuquerque, namely ALQ and ANMO, indicate identical directions for the arrival of the 26-sec energy.

CROSS SPECTRUM AZIMUTHS

The third method for determining the azimuth from each station follows (Haubrich *et al.*, 1963; Munk *et al.*, 1963). First, calculate the cross-spectral density function between the horizontal components and the vertical. The cross-spectral density function, which will be complex in general, is given by

$$G_{HZ}(P) = C_{HZ}(P) - jQ_{HZ}(P). \tag{3}$$

$C_{HZ}(P)$ is the coincident spectral density function between the horizontal and the vertical component, and $Q_{HZ}(P)$ is the quadrature spectral density function between

these two components. For a pure Rayleigh wave, the coincident spectral density term is zero. This is true because horizontal Rayleigh wave components are 90° out of phase with the vertical: the quadrature cross-spectral density term pertains to the 90° out-of-phase component in the two sets of data (Bendat and Piersol, 1971,

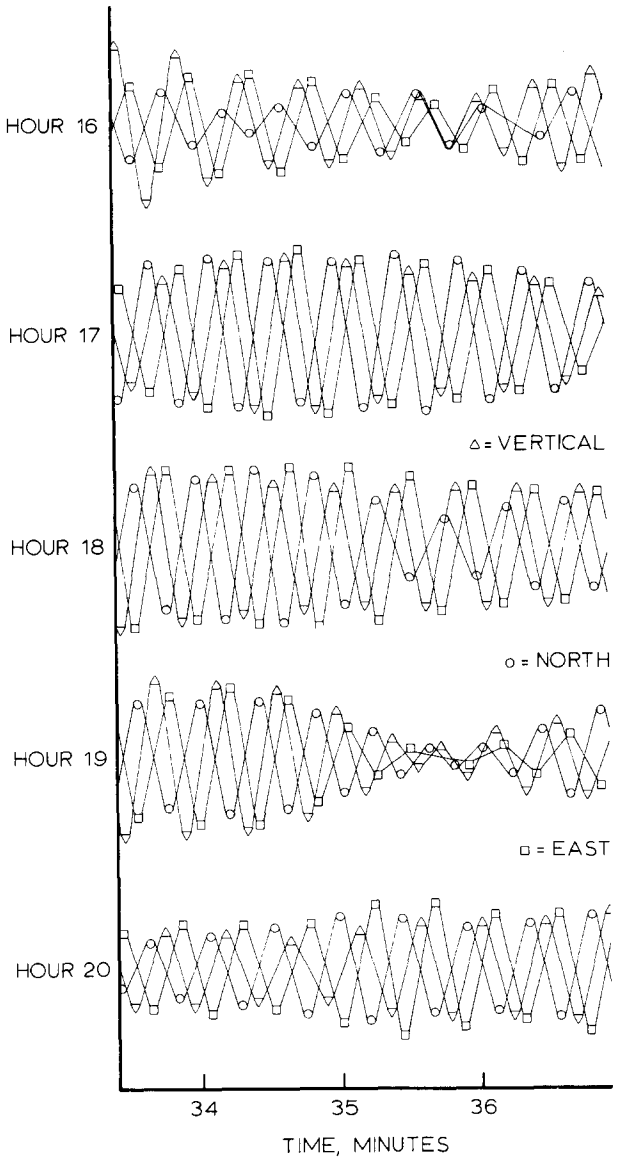

FIG. 5. Typical OGD particle motion from Day 159, 1977, for the hours shown, which indicates that Rayleigh waves are arriving from the southeast.

p. 32). Next, the amplitude cross spectrum is given by

$$A_{HZ}(P) = \sqrt{C^2_{HZ}(P) + Q^2_{HZ}(P)}, \tag{4}$$

and the cross-spectral azimuth is

$$\beta(P) = \tan^{-1} \frac{A_{NZ}(P)}{A_{EZ}(P)}. \tag{5}$$

However, $C_{HZ}(P)$ contains no information about the desired Rayleigh wave azimuth; it is either zero, or it contains part if not all of the non-Rayleigh wave portion of the amplitude spectra. Therefore, the calculated Rayleigh azimuth is more accurate if any nonzero $C_{HZ}(P)$ terms are dropped to yield

$$\beta(P) = \tan^{-1} \frac{Q_{NZ}(P)}{Q_{EZ}(P)}. \tag{6}$$

A measure of the purity of the Rayleigh wave being analyzed can be obtained by applying an expression derived from the standard coherence function. The coherence function between the north and vertical components is given by

$$\gamma^2_{NZ}(P) = \frac{|G_{NZ}(P)|^2}{G_Z(P)G_N(P)} \leqq 1, \tag{7}$$

where $G_Z(P)$ and $G_N(P)$ are the power spectral density functions for the vertical

TABLE 3

RESULTS OF PARTICLE MOTION STUDIES OF DIGITALLY BAND-PASSED DATA ASSUMING RAYLEIGH WAVE MOTION

Station	Z	N	E	Arriving Quadrant
ANMO	T*	↑	↓	SE
EIL	P	↓	↓	SW
KON	P	↓	↓	SW
MAIO	P	↓	↓	SW
OGD	T	↑	↓	SE

* T denotes trough, P denotes peak, and arrows denote earth motion in the indicated direction.

and north components, respectively. For a pure Rayleigh wave, $|G_{NZ}(P)|^2$ becomes $Q^2_{NZ}(P)$. Substituting and writing the corresponding coherence function between the east and the vertical, yields

$$\frac{Q^2_{NZ}(P)}{G_Z(P)G_N(P)} \leqq 1 \quad \text{and} \quad \frac{Q^2_{EZ}(P)}{G_Z(P)G_E(P)} \leqq 1. \tag{8}$$

Adding and rearranging yields

$$\frac{Q^2_{NZ}(P) + Q^2_{EZ}(P)}{G_Z(P)\{G_N(P) + G_E(P)\}} \leqq 1. \tag{9}$$

For a pure Rayleigh wave arriving at the station from only one direction, this expression will be equal to one. Multiple arrivals or non-Rayleigh wave motion will degrade the figure. Therefore, this modified coherence factor acts as a Rayleigh wave quality-factor.

The cross-spectral technique was applied to the 26-sec microseism storm to determine the azimuth of the arriving energy and to obtain estimates of the reliability of the calculated angles. Two days of data were analyzed in 4096-sec segments followed by nine-point frequency smoothing. Such an analysis should detect any movement in the source and should also provide a measure of the scatter in the data.

Figure 6 is an example of the results of cross spectral analysis of the data from OGD. The *upper* plot is the azimuthal spectrum in degrees north of east; the *lower* plot is the quality-factor spectrum. The quality-factor indicates negligible Rayleigh wave content in the seismic ground motion throughout the entire band with the exceptions of the narrow region centered about a period of approximately 26 sec. Here the quality-factor reaches as high as 0.95 (1.00 is a perfect single-angle Rayleigh wave). This indicates that almost all of the energy arriving in the small subband is Rayleigh wave energy arriving in a very narrow azimuth band. The azimuthal spectrum plotted in the *upper* part of Figure 6 is rather random over the entire band except for that portion in which the quality-factor spectrum is high. In this small subband, the azimuth angle reaches a reasonably constant value indicating that most of the energy in the subband is arriving from that direction. Figure 6 is typical of the results obtained from the cross-spectral analysis of data from ANMO, ALQ, EIL, KON, and MAIO, although the quality-factor is not always as high as

TABLE 4

COMPARISON OF AMPLITUDE AND CROSS SPECTRUM-DERIVED 26-SEC STATION BEARINGS WITH THE GREAT CIRCLE AZIMUTH TO THE GEOGRAPHIC POINT DESCRIBED BY LATITUDE 32° S, LONGITUDE 9° E

Station	Amplitude Spectrum Azimuth (deg)	Cross Spectrum Azimuth (deg)	Bearing to 32°S 9°E (deg)	Amplitude Spectrum Error (deg)	Cross Spectrum Error (deg)
ALQ	109	100	106	+3	−6
ANMO	109	100	106	+3	−6
CTAO	221	~*	219	+3	~
EIL	206	202	204	+2	−2
GUMO	~	~	~	~	~
KAAO	~	~	~	~	~
KIP	132	~	135	−3	~
KON	219	202	180	+39	+22
MAIO	212	214	221	−9	−7
NWAO	217	~	233	−16	~
OGD	120	118	119	+1	−1
SNZO	~	~	~	~	~
ZOBO	148	~	118	+30	~

* ~, no data.

shown in the figure. The quality-factor is generally low, except for the peak at 26 sec, and the azimuth spectrum indicates random directions except near 26 sec.

The first 2 days of storm data from ANMO, ALQ, EIL, KON, MAIO, and OGD were analyzed by the cross-spectral technique to search for changes in the indicated azimuth as a function of time. Data from the remaining stations were not processed due to the significantly smaller amplitudes of the 26-sec ground motion at the remaining stations. Figure 7 shows the calculated azimuths for ANMO, EIL, MAIO, and OGD. The results for ALQ and KON are not shown in the figure because they would overlay the plots of the ANMO and EIL data, respectively. However, data from these two stations display the same character as those presented. The cross-spectral azimuth data indicate that the source did not move significantly during the 2 days of analysis. The azimuth is especially constant during the first day of the storm: larger variations in the azimuth during the second day are probably due to the decrease in the amplitude of the microseismic ground motion and interference from small, distant earthquakes. The cross-spectral azimuths are also tabulated in Table 4; agreement with the amplitude spectrum azimuths is excellent.

The azimuthal error angles of Table 4 ignore refraction effects. Surface-wave refraction can be quite large for certain propagation paths, as has been demonstrated by Capon (1970) and Sobel and von Seggern (1978). The errors indicated in Table 4 are well within the error which might be introduced by assuming great circle propagation. Although the geographic point latitude 32° S, longitude 9° E lies at sea in deep water, a great circle model is not accurate enough to guarantee that the source is not on the nearby African coast or inland for that matter. However, the accuracy should assure that the source lies in the southeast Atlantic Ocean region.

A measure of the spread in the azimuth data is indicated by the widths of the beam patterns in Figure 8. The beams are constructed by including 90 per cent of the azimuths as determined by the cross-spectral method from 2 days of data taken 1 hr at a time.

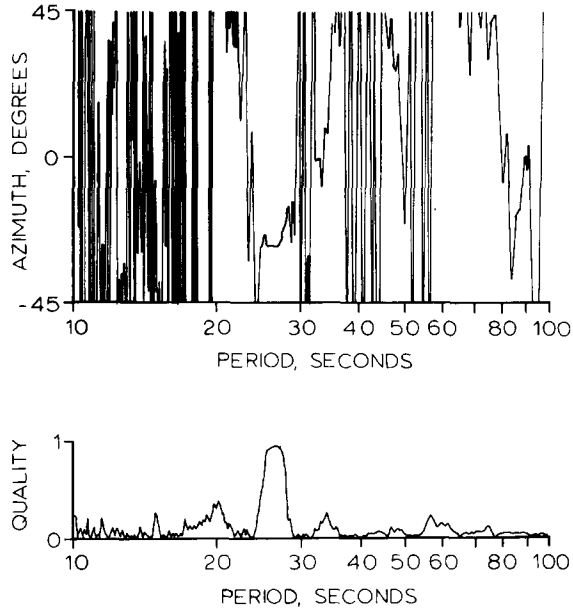

FIG. 6. Cross spectrally-derived OGD azimuth in degrees north of east. Quality factor indicates that Rayleigh waves dominate the spectrum near 26 sec.

DISPERSION

The characteristics of the June 8, 1977 storm discussed here are not significantly different from those described by Oliver (1962, 1963). Both storms appear to have originated in approximately the same geographic area, have energy concentrated in remarkably narrow bandwidth, have similar amplitude histories, and were observed worldwide. However, an important difference will become evident as the dispersion of the June 8 storm is examined. First, let us review current microseism dispersion theory.

Two previous papers on microseisms with periods close to those measured here reported dispersion which was essential to the explanation of the sources of the microseisms (Oliver, 1962; Haubrich *et al.*, 1963). Dispersion in the measured ground motion has also been observed in shorter period microseismic storms as documented by Darbyshire (1950), Oliver and Ewing (1957), Oliver and Page (1963), and Dinger (1963), among numerous others. Microseismic dispersion was attributed to dispersion in the ocean, prior to converting ocean-wave energy to seismic energy, as predicted by classical deep-water wave-propagation theory. Only the essentials of deep-ocean dispersion theory will be reviewed here (for a detailed treatment, see

Munk *et al.*, 1963). Assume that a time-and-space localized meteorological storm generates broad-spectrum ocean-wave energy at geographic point A. Classical deep-water theory predicts that the period of waves observed at point B located a distance X from A is

$$P\alpha\frac{X}{T}, \tag{10}$$

where T is the time interval between the occurrence of the storm and the time of observation. Therefore, if the observer remains at point B sufficiently far from A, he will experience narrow-band long-period ocean waves, which shift to shorter periods with time. Now, if a mechanism for converting ocean-wave energy to seismic energy exists at point B, the microseisms will be narrow-banded with dispersion. This dispersion model theoretically explains the behavior of most of the microseism storms reported in the literature.

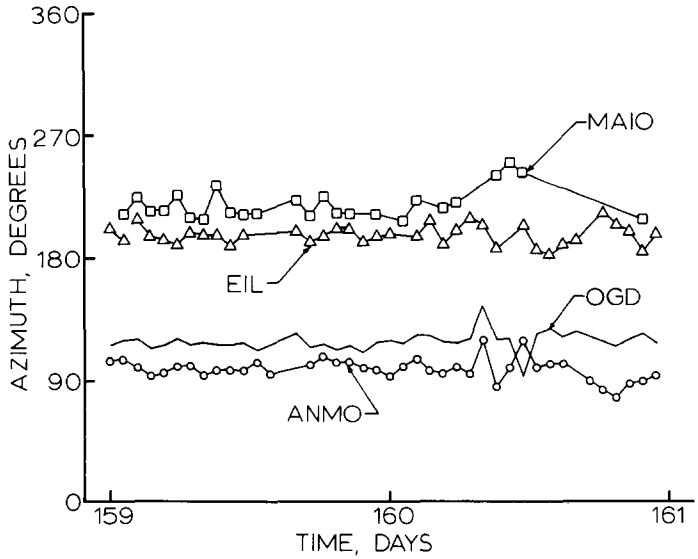

FIG. 7. Cross spectrally-derived azimuths at ANMO, EIL, MAIO, and OGD during the first 2 days of the 26-sec storm.

The dispersion of the June 8, 1977 storm was examined by calculating the power spectra for 1-hr-long segments continuously over the 4-day duration of the storm. The period at which the 26-sec energy reached its peak was determined for each time segment and then plotted as a function of time. Figure 9 compares ANMO vertical dispersion data with the dispersion reported by Oliver (1962). It is evident that a significant disparity exists between the present microseismic storm data and those reported by earlier authors. The June 8, 1977 storm contained no dispersion at all; the period of the 26-sec peak is absolutely constant during the entire 4-day duration of the storm. The same behavior is exhibited by the data from the remaining stations worldwide, as illustrated by the vertical data from the 10 stations in Figure 10. The period of the horizontal data from all of the 10 stations is also constant throughout the storm. Although not shown in detail, the shape of the spectral line does not change significantly with time. There is a slight increase in the half-power bandwidth with time (it increases from 1.74 to 1.99 sec during the first 48 hr of the storm), but since this increase is approximately symmetrical about

the central constant period of the line, it is believed to be due to the decrease of the line amplitude with respect to the constant background noise level. The lack of dispersion and the constancy of the spectral line shape severely limit the number of possible explanations for sources of the disturbance. In particular, deep-water dispersion of atmospheric storm-generated ocean waves cannot be the mechanism, which is isolating the narrow-band energy.

A Second Storm

The storm of June 8, 1977 is not unique. A second microseismic storm of this type began on July 15 and continued through July 19, 1977. This storm was also recorded

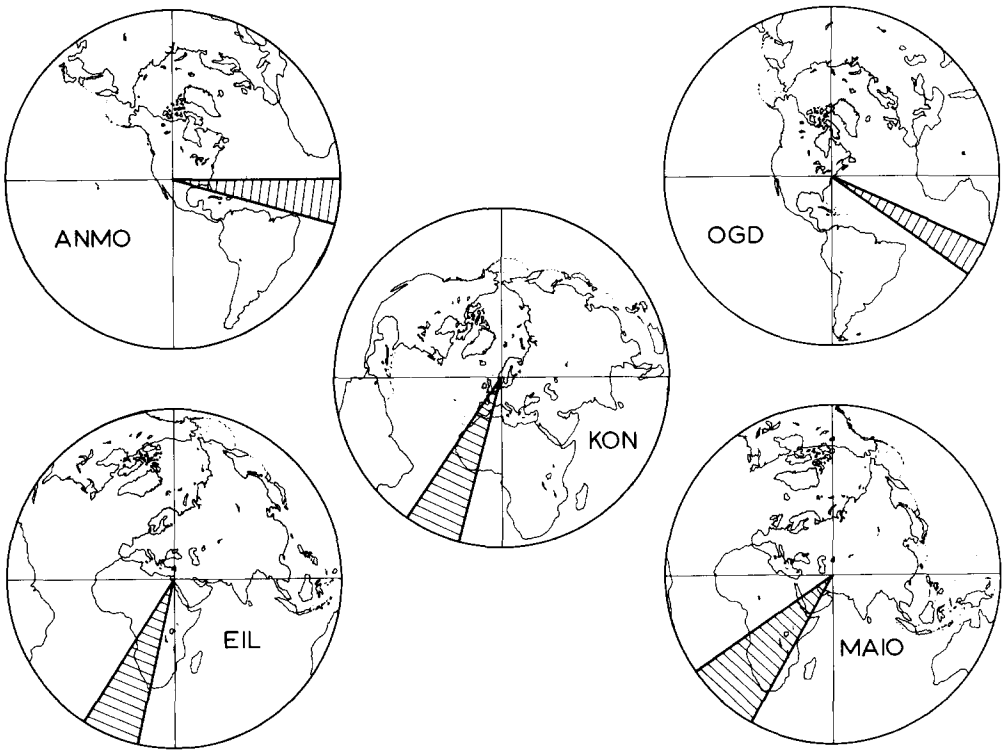

FIG. 8. Beam patterns containing 90 per cent of the cross spectrally-derived azimuths from 2 days of storm data.

worldwide with energy concentrated in a narrow bandwidth near 26 sec. The period of the data from the first storm of Table 2 is characteristic of the second storm as well. Although the second storm has not been analyzed in as much detail, indications are that the energy originated in approximately the same geographic area. Finally, the period of the spectral peak is constant throughout the over 4-day duration of the storm, proving that the nondispersive character of the first storm was not a singular example.

Discussion

Both previous studies of ultralong-period microseisms (Oliver, 1962; Haubrich *et al.*, 1963) reported clear-cut dispersion in the narrow-band seismic energy. They are well documented and contain rigorous analysis of their respective data; both papers indicate deep-water wave propagation as the source of the dispersion. The lack of

dispersion in the storm data presented here is a significant departure from these earlier results. Apparently, the two types of storms are generated by different sources or at least different manifestations of the same source.

The similarity of the amplitude history of the 26-sec storm to the amplitude histories of 7- and 18-sec microseismic storms suggests that this long-period storm might arise from a similar source, that is, an atmospheric storm at sea. Two mechanisms which might conceivably be capable of converting broad-spectrum ocean-wave energy to narrow-band nondispersive seismic energy will be presented.

The first involves the refraction of wave energy by a shoal area. Suppose that broadband ocean waves are dispersively refracted in a shallow-water area and subsequently converted to seismic energy on a distant shoreline suitably positioned to intercept only a narrow portion of the total refracted beam. The beach could subtend only that angle containing the bandwidth of energy measured in the microseisms. This mechanism requires that the atmospheric source storm remain relatively stationary in order that energy can be refracted at the proper angle to maintain constant period waves at the shoreline. A similar model has been used to explain locally generated, constant period microseisms on Aruba (Wilson *et al.*, 1973). The probability that an atmospheric storm would remain in a small geographic

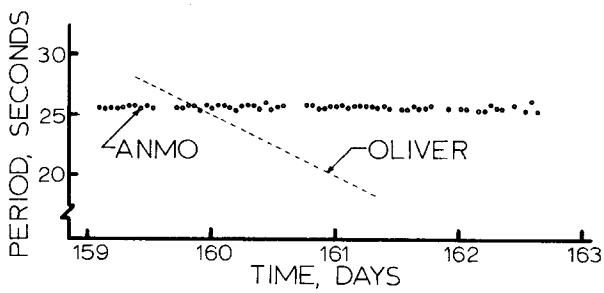

FIG. 9. Dispersion of the vertical microseismic earth motion at ANMO. Dashed line approximates the dispersion rate obtained by Oliver (1962).

area for several days as required by the 26-sec microseismic storm data is not great. However, it appears that microseismic storms of this intensity are infrequent because several years of long-period data have been examined during which only two large storms have been found. Several smaller storms occurred, but apparently the proper conditions required for the generation of large 26-sec microseisms are rare.

The narrow-band, constant period character of the 26-sec microseism storms suggests a resonance phenomenon. Oceanic edge waves on the coast of Africa may provide a resonance mechanism which could generate such ground motion. Recent studies (Huntley, 1976; Bowen and Guza, 1978) have indicated that edge waves whose period corresponds to the cutoff frequency of the beach as determined by the physical parameters of the beach may be strongly resonant. If resonant edge waves are generated along extended sections of Africa's relatively uniform southwest coast during extraordinary oceanic storms, they could be the source of the exceptionally large microseismic peak. Excitation of resonant edge waves along shorter sections of the coast during ordinary oceanic storms could be the source of the lower levels of 26-sec energy which persists in the background spectrum worldwide. Unfortunately, the complexities of geography, shoreline profiles, and the many possible weather system distributions make a mathematical analysis of the feasibility of resonant edge-wave generation exceedingly difficult.

The intricateness of the models presented above suggests that the source of nondispersive seismic energy may not lie in the atmospheric storm-ocean system. If it does not, it would be quite significant, but speculating on possible nonocean models based on the currently available data would be even more tenuous.

In an effort to determine the presence of an ocean-storm source, meteorological satellite photographs have been examined for abnormal oceanic storms in the South Atlantic regions. In addition, both the Southern Hemisphere surface and 500 mbar synoptic charts, as prepared by the Bureau of Meteorology in Melbourne, Australia, have been studied in conjunction with the satellite photographs. There appears to be nothing abnormal about the weather in the South Atlantic during the month centered on the microseismic storm. A complex system of low-pressure centers constantly circled the Antarctic continent, but the lows in the area show no abnormal severity during the time period. However, both models discussed above require that any generating storms be suitably positioned with respect to geographic features; such special conditions would be difficult to isolate by visual observation.

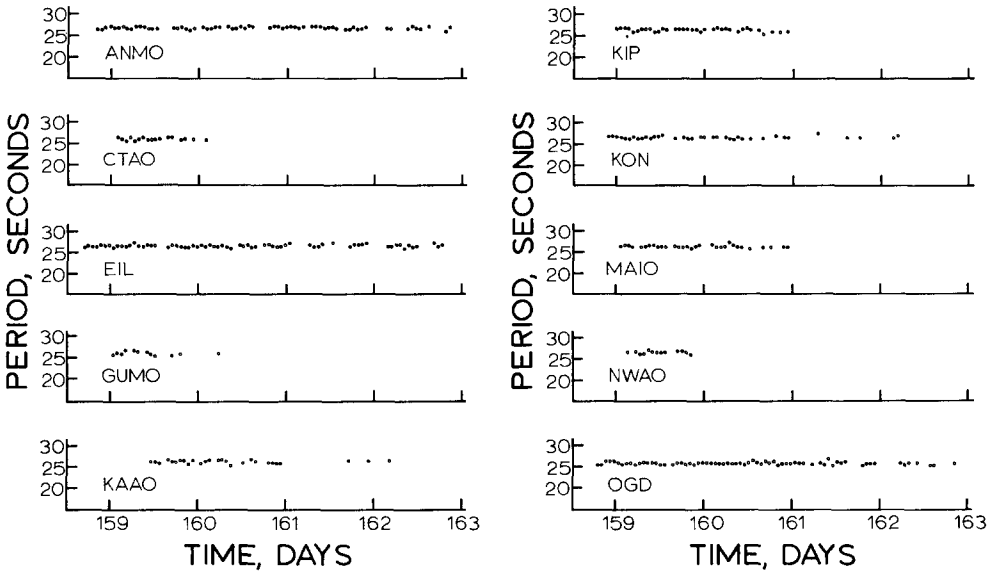

FIG. 10. Vertical dispersion data from the stations indicated. Gaps are caused by interference by earthquakes.

CONCLUSIONS

A narrow-band peak exists in the background earth motion spectrum in the region of 26 sec. This peak persists throughout time and occasionally increases to large amplitudes during isolated nondispersive storms. The lack of dispersion eliminates deep-water wave propagation as the explanation for the narrow-band energy. Future analysis will be aimed at identifying the mechanism responsible for the 26-sec earth motion.

ACKNOWLEDGMENTS

The author is indebted to Jon Peterson and Jim Murdock (Albuquerque Seismological Laboratory) for helpful discussions during this investigation and to Bob Sheppard (Lincoln Laboratory) for providing the station-centered maps used in Figure 8. The digital data on which these results are based were recorded by the HGLP, ASRO, and SRO stations operated by the Albuquerque Seismological Laboratory.

REFERENCES

Bendat, J. S. and A. G. Piersol (1971). *Random Data: Analysis and Measurement Procedures*, Wiley-Interscience, 328 pp.

Bowen, A. J. and R. T. Guza (1978). Edge waves and surf beat, *J. Geophys. Res.* **83,** 1913–1920.

Capon, J. (1970). Analysis of Rayleigh-wave multipath propagation at LASA, *Bull. Seism. Soc. Am.* **60,** 1701–1731.

Darbyshire, J. (1950). Identification of microseismic activity with sea waves, *Proc. Roy. Soc., (London), Ser. A* **202,** 439–448.

Dinger, J. E. (1963). Comparison of ocean-wave and microseism spectrums as recorded at Barbados, West Indies, *J. Geophys. Res.* **68,** 3465–3471.

Evernden, J. F. (1953). Direction of approach of Rayleigh waves and related problems (part 1), *Bull. Seism. Soc. Am.* **43,** 335–357.

Evernden, J. F. (1954). Direction of approach of Rayleigh waves and related problems (part 2), *Bull. Seism. Soc. Am.* **44,** 159–184.

Haubrich, R. A., W. H. Munk, and F. E. Snodgrass (1963). Comparative spectra of microseisms and swell, *Bull. Seism. Soc. Am.* **53,** 27–37.

Huntley, D. A. (1976). Long-period waves on a natural beach, *J. Geophys. Res.* **81,** 6441–6449.

Iyer, H. M. (1964). The history and science of microseisms. *Vesiac State-of-the-Art Report 4410-64-X*, Institute of Science and Technology, University of Michigan, Ann Arbor, Michigan.

Munk, W. H., G. R. Miller, F. E. Snodgrass, and N. F. Barber (1963). Directional recording of swell from distant storms, *Phil. Trans. Roy. Soc. London, Ser. A*, **255,** 505–584.

Oliver, J. (1962). A worldwide storm of microseisms with period of about 27 seconds, *Bull. Seism. Soc. Am.* **52,** 507–517.

Oliver, J. (1963). Additional evidence relating to "a worldwide storm of microseisms with period of about 27 seconds," *Bull. Seism. Soc. Am.* **53,** 681–685.

Oliver, J. and M. Ewing (1957). Microseisms in the 11 to 18 second period range, *Bull. Seism. Soc. Am.* **47,** 111–127.

Oliver, J. and R. Page (1963). Concurrent storms of long and ultralong period microseisms, *Bull. Seism. Soc. Am.* **53,** 15–26.

Simons, R. S. (1968). A surface wave particle motion discrimination process, *Bull. Seism. Soc. Am.* **58,** 629–637.

Sobel, P. A. and D. H. von Seggern (1978). Application of surface-wave ray tracing, *Bull. Seism. Soc. Am.* **68,** 1359–1379.

Wilson, W. S., D. G. Wilson, and J. A. Michael (1973). Analysis of swell near the island of Aruba, *J. Geophys. Res.* **78,** 7834–7844.

U.S. GEOLOGICAL SURVEY
ALBUQUERQUE SEISMOLOGICAL LABORATORY
BLDG. 1002, KIRTLAND AFB-EAST
ALBUQUERQUE, NEW MEXICO 87115

Manuscript received May 30, 1979